ECS Transactions, 16 (2) 159-170 (2008)
10.1149/1.2981852 ©The Electrochemical Society

Polyaniline-derived Non-Precious Catalyst for the Polymer Electrolyte Fuel Cell Cathode

Gang Wu[a], Zhongwei Chen[a], Kateryna Artyushkova[b], Fernando H. Garzon[a], and Piotr Zelenay[a]

[a] Materials Physics and Applications Division, Los Alamos National Laboratory, Los Alamos, New Mexico 87545, USA
[b] Department of Chemical and Nuclear Engineering, University of New Mexico, Albuquerque, New Mexico 87131, USA

This paper focuses on a new polyaniline-derived non-precious cathode catalyst with high oxygen-reduction activity, verified in electrochemical and fuel cell testing. The rotating disk (RDE) onset and half-wave potential ($E_{½}$) of oxygen reduction were measured at 0.90 V and 0.77 V, respectively. Rotating ring-disk electrode (RRDE) study revealed very good selectivity in the four-electron reduction, with H_2O_2 yields below 1% (0.4% at 0.4 V). Similarly, the catalyst showed good performance in the hydrogen-air fuel cell, even at high cell operating voltages, yielding 0.04 A cm^{-2} at 0.80 V and 0.21 A cm^{-2} at 0.6 V. Fuel cell life test at a constant voltage of 0.4 V demonstrated promising stability up to 450 hours, generating a current density of approximately 0.32 A cm^{-2}, a respectable performance for a non-precious cathode catalysts operated on air rather than oxygen. *Ex situ* characterization pointed to pyridinic- and pyrrolic-nitrogen metal species as likely active ORR sites.

Introduction

The development of non-precious catalysts with high activity and practical durability in the oxygen reduction reaction (ORR) have become a major focus area for the polymer electrolyte fuel cell (PEFC) research as a way of potentially reducing the currently prohibitive PEFC cost. During several decades of research effort in non-precious metal electrocatalysis, a significant progress has been achieved in the synthesis, performance improvement, and understanding of the ORR mechanism (1-3). Among many attempted catalyst formulations, macrocycle complexes of transition metals, pyrolyzed at 500-1000°C in an inert atmosphere (4, 5) are known for their catalytic activity toward oxygen reduction in acid media. The pyrolysis process was proposed to partially or completely break down the macrocyclic ring, resulting in new materials with ORR activity influenced by the precursors employed. In an effort to explore this kind of novel pyrolyzed non-Pt catalysts, different catalysts have been prepared in a similar manner, using a wide variety of N-containing chemicals as the starting materials, many of which no longer macrocyclic. Even though it is generally accepted that, at least partially destructive, heat-treatment step is needed for catalyst activity and stability improvements, the enhanced performance of the catalysts remains strongly dependent on the synthesis methods, carbon support used, the source of metal and nitrogen, and the thermal treatment conditions. In general, the nature of ORR active sites on such-fabricated catalysts has not been unambiguously determined, remaining the subject of much debate

that concentrates on the roles of the metal in the formation of active catalytic sites. While Dodelet et al. (6) provided data indicating that the active site involves MeN_x/C-type species (Me: Co and Fe), other researchers (7-9) suggested that, rather than participating directly in active sites for ORR, transition metals play a role in the formation of such sites by catalyzing nitrogen-doping of the graphitic carbon during the pyrolysis step. These authors tied ORR activity to various nitrogen functionalities (pyridinic or quaternary nitrogen) on the carbon surface.

In this work, a new oxygen-reduction non-precious catalyst was developed by polymerizing aniline on the surface of carbon black nanoparticles and heat-treating thus obtained layered "hybrid" materials in the presence of Fe- and/or Co- species. One of the advantages of using polyaniline (PANI) is that it can act both as the carbon source and nitrogen precursor, potentially facilitating the formation of nitrogen-containing sites on the graphitic carbon surface during the catalyst synthesis. Various transition metals such as Fe and Co were used in the synthesis, with ensuing catalysts studied for ORR activity and four-electron selectivity. The catalysts were also systematically characterized using both electrochemical and physical techniques to explore the roles of each element (C, N, Co and Fe) and possible active sites.

Experimental Details

Synthesis of PANI-derived catalysts

In situ polymerized aniline, chelated with transition metals (Fe and Co), was deposited onto carbon supports, followed by the pyrolysis step. Carbon black, typically a commercial Ketjen Black EC 300J (10) with BET surface area of about 950 $m^2 g^{-1}$ and good corrosion resistance, was ultrasonically dispersed in the 0.5 M HCl solution. The suspension was kept below 10°C while the aniline and the oxidant reagent, ammonium peroxydisulfate in 0.5 M HCl, was added drop-wise under constant stirring. After 12 hours, the transition metal salts, such as $FeSO_4 \cdot 7H_2O$ and $CoSO_4 \cdot 6H_2O$, were added to the suspension to form a complex with polyaniline coated onto carbon black. The carbon-supported PANI-Me (Me = Fe or Co) was vacuum-dried using a rotary evaporator. The subsequent heat-treatment was performed at 900°C in an inert atmosphere of a nitrogen gas for 1 hour. The pyrolyzed sample was subsequently pre-leached in 0.5 M H_2SO_4 at 80°C for 8 hours and then fully washed in de-ionized water (9). The product was a PANI-derived non-precious catalyst, denoted here as PANI-Me-C.

In order to explore the role of nitrogen and transition metals in ORR catalysis, the performance of various catalysts synthesized in this study has been related to that of the carbon black (denoted as carbon) and polyaniline-coated carbon (denoted as PANI-C) control samples. These samples were subject to the same pyrolysis step and chemical post-treatment as the actual catalysts.

Rotating disk (RDE) and rotating ring-disk electrode (RRDE) measurements

To avoid any potential contamination of non-precious metal catalyst by platinum, all RDE/RRDE experiments were carried out using a gold mesh as the counter electrode. Also, electrochemical characterization of the catalysts was carried out on the rotating disk electrode (without the ring). The rotating ring-disk electrode, with a Pt disk, was used

subsequent to other experiments, only to determine catalyst selectivity in the four-electron process. The RDE was made of a 5.0 mm-diameter glassy carbon, while RRDE of a glassy 5.61 mm carbon disk and a Pt ring (6.25 mm inner diameter, 7.92 mm outer diameter). All RDE/RRDE measurements were performed using CHI Electrochemical Station (Model 750b) in a conventional three-electrode cell with 0.5 M H_2SO_4 electrolyte at room temperature. An Ag/AgCl electrode in 3.0 M NaCl (0.209 V vs NHE) was used as a reference electrode. All potentials were then converted to the NHE scale. To deposit the catalyst onto the disk electrodes, a 10.0 mg catalyst sample was ultrasonically dispersed in 1.0 ml ethanol solution for 30 min to form a catalyst "ink". Then, 15 μl of the ink and 5 μl of a 5% Nafion® solution were applied to the glassy-carbon disk. In RDE tests, the background capacitive currents were recorded in a potential range from 1.0 V to 0.0 V in nitrogen-purged electrolyte at a scan rate of 5 mV s^{-1}. Then, solutions were saturated with oxygen, followed by a cathodic linear sweep voltammetry (CLSV) at the same scan rate of 5 mV s^{-1}. The disk rotation rate was 900 rpm. The oxygen reduction current was corrected for the background current to yield ORR activity of the tested catalysts. Voltammetric scans were typically recorded in the potential range from 1.0 to 0.0 V.

In RRDE testing, the ring potential was set to 1.2 V. Before experiments, the Pt catalyst in the ring was activated by potential cycling in 0.5 M H_2SO_4 from 0 to 1.4 V at a scan rate of 50 mV s^{-1} for 10 minutes. Four-electron selectivity of catalysts was evaluated based on H_2O_2 yields, calculated from the following equation (11).

$$H_2O_2(\%) = 200 \times \frac{I_R / N}{(I_R / N) + I_D} \qquad [1]$$

Where, I_D and I_R is the disk and ring current, respectively, and N is the ring collection efficiency constant.

Fuel cell testing

PANI-derived non-precious catalysts were tested at the fuel cell cathode to evaluate their activity and durability under PEFC operating conditions. Catalyst inks were prepared by ultrasonically mixing catalyst powders with Nafion® solution for four hours. Cathode inks were applied to the gas diffusion layer (GDL, ELAT LT 1400W, E-TEK) Catalyst application process continued until the cathode catalyst loading reached 4 mg cm^{-2}. The Nafion® content in the dry catalyst was 30 wt%. A commercially-available Pt-catalyzed cloth GDL (E-TEK, 0.25 mg/cm^2 Pt) was used for the anode.

The cathode and anode electrode were hot-pressed onto two separate pieces of a Nafion® 1135 membrane, later put together to form a two-layer MEA. This approach minimized the risk of a possible cross-contamination of the cathode with platinum from the anode and also greatly facilitated *post mortem* characterization of individual fuel cell electrodes. The geometric area of the MEA was 5.0 cm^2. Fuel cell testing was carried out in a single cell with serpentine flow channels. Pure hydrogen and air/oxygen humidified at 85°C were supplied to the anode and cathode at a flow rate of 200 and 600/400 mL/min, respectively. Both electrodes were maintained at the same backpressure of 30 psig (~40 psi absolute pressure at the Los Alamos altitude). Fuel cell polarization plots were recorded using standard fuel cell test stations (Fuel Cell Technologies Inc.). Recorded voltage data, obtained with the two-membrane sandwich were corrected for the

resistance of one of the membranes, which means that all fuel cell polarization data presented in this paper correspond to an MEA with a single Nafion® 1135 membrane. Fuel cell life testing was carried out at a constant voltage of 0.4 V.

Physical characterization

High-resolution transmission electron microscopy (HR-TEM) images were taken on a Philips TECNI12 microscope operating at 200 kV. X-ray photoelectron spectroscopy (XPS) was performed on a Kratos Axis Ultra spectrometer using a Mg Kα X-ray source ($h\nu$ =1253.6 eV) with primary tension of 12 kV and emission current of 20 mA. The crystallinity of various samples was determined by X-ray diffraction (XRD) using a Bruker D5000 diffractometer with Cu Kα radiation ($\lambda_{K\alpha l}$=1.5418 Å). X-ray fluorescence spectroscopy Thermo Scientific QuanX (XRF) was also employed to analyze the metal contents in catalysts.

Results and discussion

Electrochemical and fuel cell performance of PANI-derived catalysts

RDE and RRDE testing. ORR activity and four-electron selectivity data for various samples, including four controls (as-received carbon, pyrolyzed carbon black, pyrolyzed PANI-C, and Pt/C catalyst) in 0.5 M H_2SO_4 are shown in **Figure 1**. While pyrolysis leads to an improvement in the ORR activity of carbon (Ketjen Black EC 300J), resulting in a positive shift in the ORR onset potential when compared with as-received carbon, both carbon samples exhibit poor ORR performance and suffer from high peroxide yields relative to the best-performing catalysts. This indicates that, whether heat-treated or not, the carbon surface provides few active sites for oxygen reduction, mainly to H_2O_2 on a two-electron path. Similar results were reported before for other carbon materials, Vulcan XC-72 and Black Pearl 2000 (12).

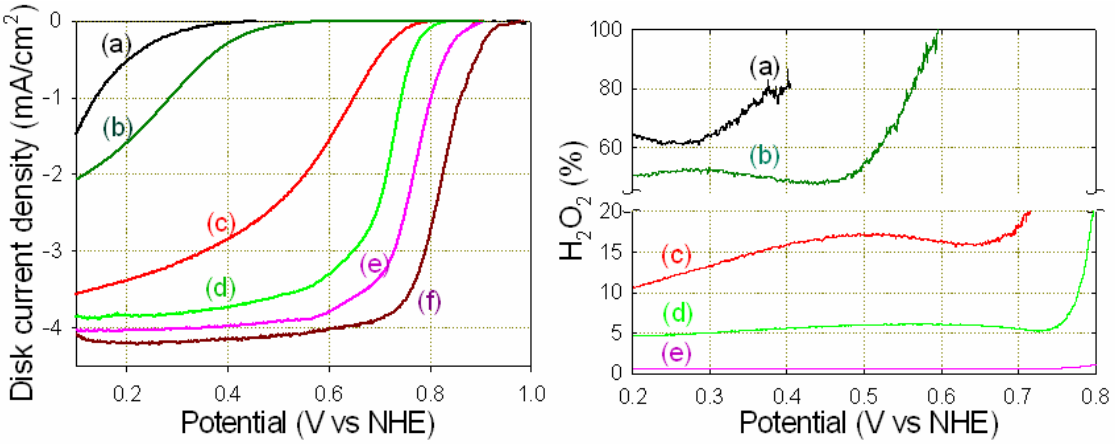

Figure 1. RDE polarization plots (left) and RRDE H_2O_2 yields (right) recorded with various catalysts in 0.5 M H_2SO_4: (a) as-received carbon black; (b) pyrolyzed carbon black; (c) PANI-C; (d) PANI-Co-C; (e) PANI-FeCo-C; (f) E-TEK Pt/C catalyst (Pt loading: 0.06 mg cm^{-2}). See Experimental Details for additional information.

In the case of pyrolyzed PANI-coated carbon, the introduction of nitrogen with PANI leads to a significant improvement in activity, evidenced by the positive shifts of

the onset ORR potential onset from 0.52 to 0.79 V and of the half-wave potential from 0.28 to 0.60 V. At the same time, the H_2O_2 yields decrease to 16% at 0.40 V. XPS, electronic structure probes, and density functional theory (13) suggested earlier that carbon atoms may be substituted by nitrogen atoms in the pyrolysis forming N-doped carbon structures, mainly in the forms of pyridinic and quaternary nitrogen. Thus, the nitrogen-doped carbon with N-C and N=C bonds on surface appears to facilitate oxygen reduction at carbonaceous materials. Such sites appear unable to fully promote the four-electron reduction process.

Addition of transition metals to the PANI-Me-C catalyst dramatically improved the activity and selectivity of the catalyst toward oxygen reduction via four-electron reduction to H_2O. In particular, the ORR onset potential measured with PANI-Co-C shifted to 0.82 V and that of PANI-FeCo-C reached 0.90 V (**Figure 1**). At the same time, the half-wave potential values increased to, correspondingly, 0.72 and 0.77 V. Limiting current was reached in both cases, attesting to the high number and uniform distribution of ORR active sites on the surface of catalysts (14). Transition metals not only significantly improved ORR activity, but also reduced H_2O_2 yields, to 5% with PANI-Co-C and 0.4% with PANI-FeCo-C at 0.4 V. Further optimization of the Fe-to-Co ratio in the catalyst could result in even better ORR activity and selectivity.

Effect of post-treatment on ORR catalysis. Post-treatment of as-received catalysts, including pyrolysis and chemical leaching, plays a major role in achieving good performance of PANI-derived catalysts. Activity and selectivity of PANI-FeCo-C samples at different stages of the synthesis are shown in **Figure 2**. While the pyrolysis step is required for the formation of the active sites and inducing ORR activity, the removal of unstable phases from the porous catalyst surface in the acid leaching step leads to further improvement in the performance. As more active sites are likely being exposed and higher surface area with increased mass transfer are achieved, the onset potential of oxygen reduction rises by nearly 0.1 V and peroxide yield drops from ~5% to 0.4% at 0.4 V.

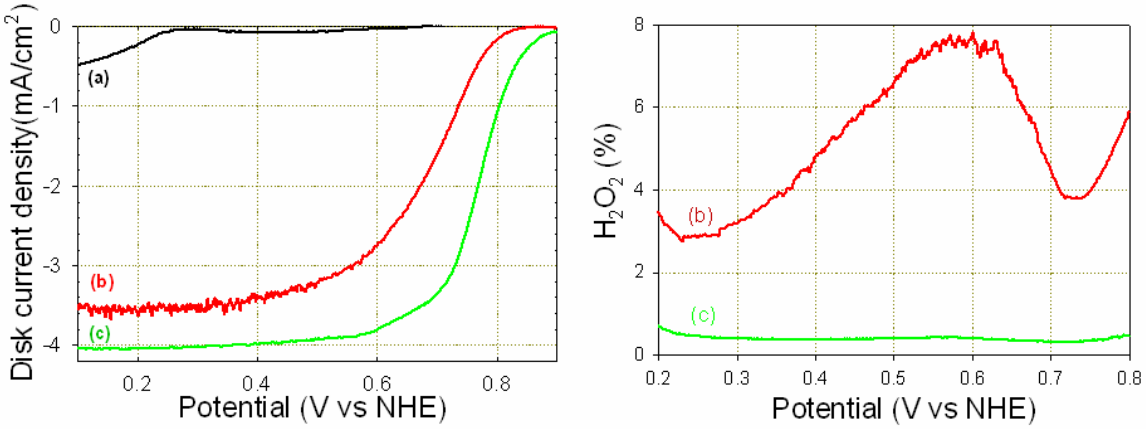

Figure 2. ORR activity and H_2O_2 yield obtained with PANI-FeCo-C catalyst at different catalyst synthesis stages (a) before pyrolysis; (b) after pyrolysis but before chemical treatment; (c) after chemical treatment.

The role of the metal content. Both the type and content of the metal play an important role in achieving high catalytic activity. Activity of the PANI-FeCo-C catalyst increases continuously with the metal content in the precursor materials, up to ~2.5 wt%

(**Figure 3**). As found by others before, the optimum transition-metal content in non-precious metal catalysts depends on the nitrogen precursor (ligand), and preparation conditions (15). Furthermore, the optimum metal content can be affected by the surface area of carbon supports. The carbon supports with high BET area, such as Ketjen black used in this work, can accommodate more active metal species, thus increasing the number of active sites. Because of a positive correlation between the half-wave potential and the metal amount observed in the case of PANI-derived catalysts, there is also a possibility that metal species could be directly related to active sites.

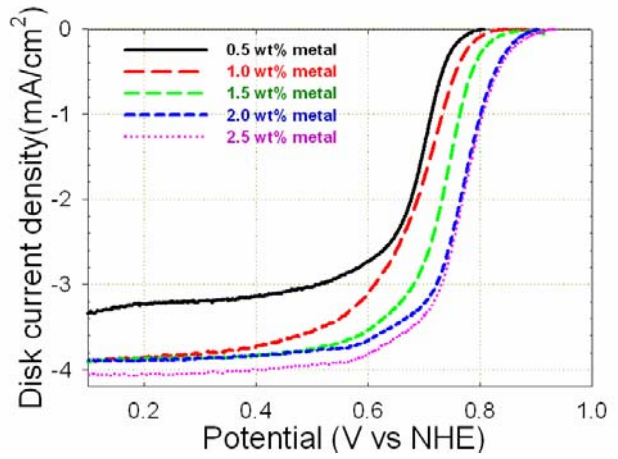

Figure 3. Effect of the metal content in the synthesis on ORR activity of various PANI-FeCo-C catalysts.

Fuel cell testing. Fuel cell polarization and life-test data recorded with a PANI-derived cathode catalyst are presented in **Figure 4(a)** and **4(b)**, respectively. The open-cell voltage values are 0.90 and 0.95 V on air and oxygen, respectively. Current density, which is a relatively low 0.04 A cm^{-2} at 0.80 V, increases to 0.21 A cm^{-2} for 0.6 V (air). Much higher performance is achieved with oxygen.

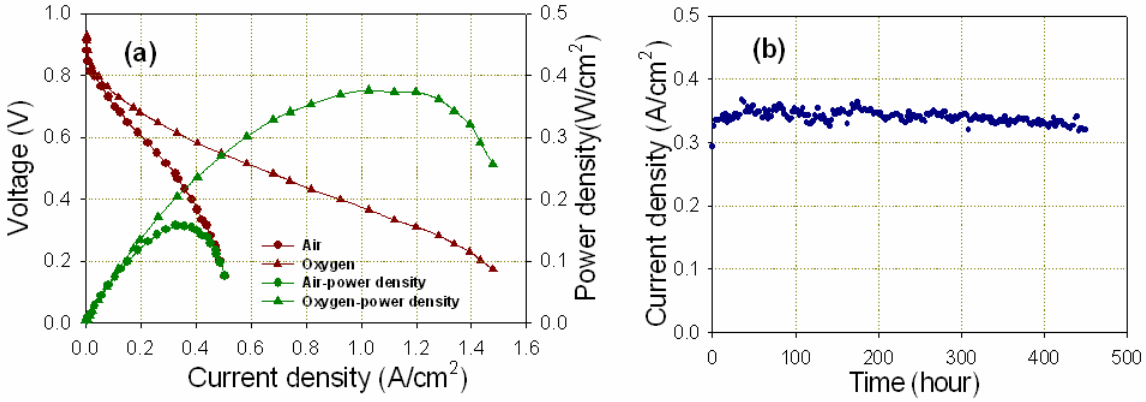

Figure 4. Fuel cell testing of a PANI-FeCo-C cathode catalyst at a loading of 4 mg cm^{-2}; cathode backpressure of 30 psig and 80^{o}C (a) polarization curves; (b) life test at 0.40 V using H_2/Air.

A 450-hour life test at a constant cell voltage of 0.40 V revealed promising stability of the MEA with non-precious PANI-FeCo-C catalyst at the cathode. No degradation was observed for the first 300 hours, followed by a slight performance loss by less than 2% relative to initial cell performance. The current density during the test was measured at

~0.32 A cm^{-2}, a respectable value for a cell with non-precious cathode, operated on air rather than oxygen.

In summary, rotating-disk and fuel cell measurements demonstrated promising activity and good stability of PANI-derived cathode catalysts for oxygen reduction. The highest activity was reached with catalysts obtained by mixing iron and cobalt precursors. Further investigation of this interesting result is planned by both electrochemical and *ex situ* characterization methods.

HR-TEM analysis

HR-TEM images of PANI-derived catalysts at different synthesis stages are shown in **Figure 5**. In Figure 5(a), carbon black particles can be seen covered by *in situ* polymerized PANI (light contrast). Pyrolysis of polyaniline-Me complexes, cf. the inset in Figure 5b, leads to the formation of metal particles surrounded by graphitic carbon shells, which are evidenced by lattice fringes. The metal particles nearly disappear after the chemical pre-leaching with sulfuric acid. Noticeably, hollow carbon nanostructures can also be seen as a result of the dissolution of metal particles from the graphitic carbon shells (Figure 5c and 5d). The electron conductivity for electrocatalysis is likely to benefit from the formation of the layers of graphitic carbon seen in HR-TEM images

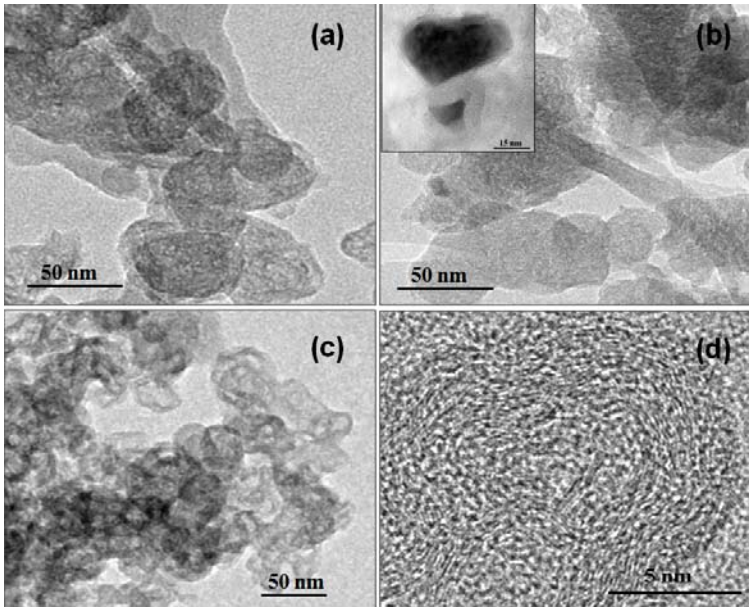

Figure 5. High-resolution TEM images of PANI-FeCo-C catalysts: (a) before pyrolysis; (b) after pyrolysis but before chemically leaching; (c), (d) after chemically leaching.

XPS analysis

N 1s spectroscopy. XPS analysis was used in this work to explore the effects of pyrolysis on the state of the catalyst surface. A comparison of N 1s spectra at different stages of the catalyst synthesis is shown in **Figure 6**. While absent for pyrolyzed carbon black, a typical N 1s spectrum is observed with polyaniline polymerized on the carbon substrate. The relatively broad peaks suggest an existence of several structures in polyaniline. The peak with the lowest binding energy (398.7 eV) is due to the imine-like

(=N–) structure, and the peak centered at 399.8 eV is attributed to the amine-like nitrogen atoms (–NH–). The peak centered at 401.6 eV can be assigned to cationic nitrogen atoms on the polymer backbone, and the peak with highest binding energy (402.8 eV) is due to the protonated amine units (16).

After the pyrolysis at 900°C under inert atmosphere, the spectrum obtained with PANI-coated carbon shows two dominant peaks at 398.7 eV and 401.2 eV. It is generally assumed that, following heat-treatment at temperatures higher than 700°C, the N 1s XPS peaks of nitrogen functional groups on carbon can be attributed to four N-species: pyridinic N (398.6±0.3 eV), pyrrolic N (400.5±0.3 eV), quaternary N (401.3±0.3 eV) and N-X (402-405 eV) (13). The N 1s spectra of the PANI-C sample thus imply that polyaniline undergoes complete decomposition at pyrolysis temperatures used in this work, with pyridinic and quaternary N species being formed at the edge and inside of graphitic carbon layers.

The pyridinic and pyrrollic peaks shift in the spectrum of the PANI-FeCo-C catalyst to 398.3 EV and 400.6 eV, respectively. Such a shift suggests possible interactions between nitrogen and metal species, accompanied by an electron transfer from the metal atoms to nitrogen atoms to form pyridinic and pyrrolic Me-N species that survive the pyrolysis step. This agrees with the reports that porphyrin-like structures are retained in the products of the pyrolysis of metal-porphyrin precursors, as found using XPS (17), XANES (18), and Mössbauer spectroscopy (19).

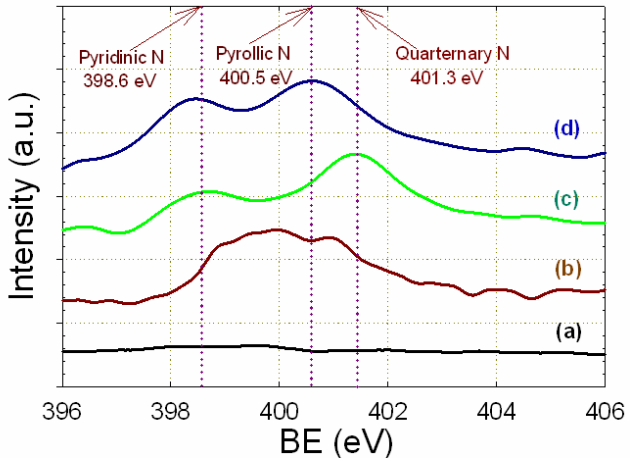

Figure 6. N 1s spectra of XPS analysis for (a) carbon; (b) PANI-coated carbon; (c) PANI-C catalysts; (d) PANI-FeCo-C catalysts.

Recently, Popov et al (9) reported a carbon composite catalyst, derived from carbon-supported complex of ethylene diamine (EDA) with Co and Fe with dominant pyridinic and quaternary nitrogen functional groups. Since no metal species were detected by XPS, the authors claimed that Co and Fe only act to facilitate the incorporation of pyridinic and graphitic nitrogen groups into the carbon matrix, which ultimately become the active catalytic sites for oxygen reduction. However, the activity and stability of PANI-derived catalyst are higher than those of the EDA-CoFe system, indicating differences in the nature of the active site in both cases, with possible involvement of the metal in the ORR process on PANI-derived catalysts. Those differences may due to the aromatic character of polyaniline, resulting in a stronger bond to the carbon support and therefore more facile electron transfer from the active metal

sites to oxygen. This is in agreement with the results by Claude et al (20) showing that heat-treated cobalt phthalocyanine (CoPc) had a higher activity than cobalt cyclam.

Co 2p and Fe 2p spectroscopy. High-resolution surveys of Co 2p and Fe 2p, shown in **Figure 7** indicate the presence of a variety of cobalt and iron species, including metals, oxides, nitrides and carbides. In Fe 2p spectra, the peak at 707 eV can be attributed to metallic Fe or Fe carbide, while peaks at 709 and 711 eV can be assigned to Fe(II) and Fe(III) species, respectively. Metallic iron and cobalt, and their oxides, supported on carbon, have been previously reported to be inactive in oxygen reduction acidic media. If so, the nature of the ORR active site remains open in both cases. One possibility is that active sites involve Fe and Co species stabilized through interaction with nitrogen and carbon, evidenced by the difference of N 1s between PANI-C and PANI-Me-C samples. Dodelet et al (21) reported a shift in the peak Fe $2p_{3/2}$ in heat-treated iron porphyrins to a lower binding energy due to the formation of aggregates at higher heat-treatment temperatures. The aggregates included Fe(0) (706.7-707.2 eV), Fe(II) (707.1-708.7 eV) and Fe carbides (706.7-706.9 eV). Using time of flight secondary ion mass spectroscopy (ToF SIMS), the same authors proposed two possible catalytic sites FeN_2/C and FeN_4/C for their Fe-N-C catalysts. These FeN_4/C and FeN_2/C species are iron ions coordinated by four nitrogen atoms of a pyrrolic type and two nitrogen atoms of a pyridinic type, respectively, bound to carbon supports (22-24).

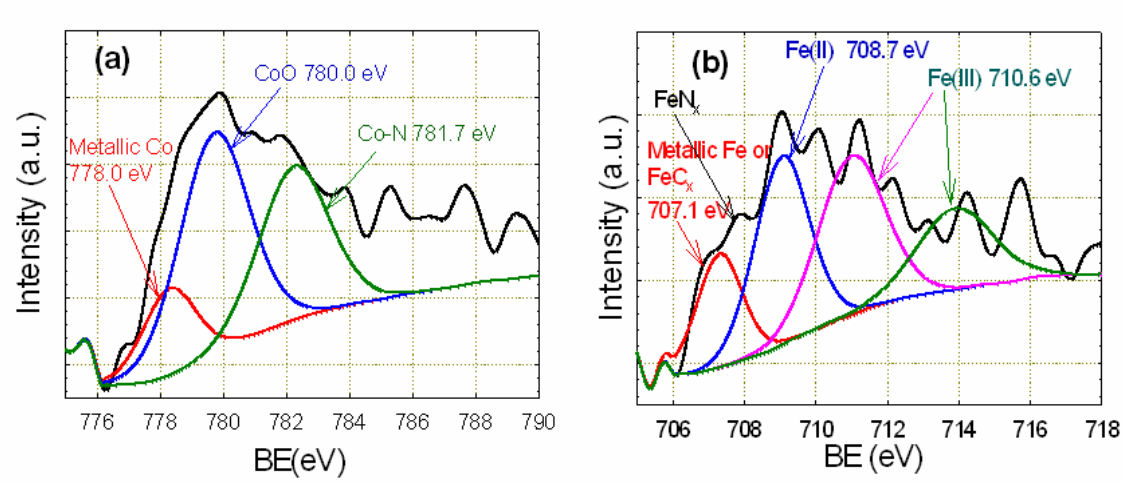

Figure 7. XPS analysis for transition metal onto PANI-FeCo-C catalyst (a) Co 2p; (b) Fe 2p.

XRD analysis

XRD patterns for various samples are summarized in **Figure 8**. As-received carbon black showed a very broad carbon (002) peaks at 2θ=25° that can be attributed to two different forms of carbon, referred to previously as turbostratic carbon (carbon black) and graphene carbon (graphitic structure) (25). Pyrolysis of carbon black led to an enhancement in the graphitic character, giving rise to a sharp peak at 25.4°. This effect was not seen with pyrolyzed PANI-C sample. Un-pyrolyzed PANI-Fe-C sample, containing 0.5 wt% of Fe, showed well-developed crystalline structures, assignable mainly to the excess of the oxidant APS (2θ=17.6°, 18.2°, 22.2°, 26.6° and 30.4°) and small amount of iron salts (2θ = 31.2°, 36 4° and 45.1°). Also seen were broad polyaniline peaks located at 16.8°, 20.4° and 24.6°. Virtual absence of peaks attributable

to iron salts suggests that Fe ions were not present in periodic structures. In the case of pyrolyzed PANI-Fe-C sample (Figure 8e), the peaks attributable to the crystalline phases can be mainly assigned to troilite FeS (2θ = 17.1°, 18.7°, 29.9°, 31.9°, 33.7°, 35.7°, 43.3°, 47.2°, 54.0°, 63.5°and 70.8°)(26), and to a lesser degree to metallic Fe (2θ = 44.8° and 64.5°). Those crystalline phases mostly disappear after the acid treatment (Figure 8f). The absence of crystalline iron-containing phases in the pyrolyzed and acid-leached PANI-Fe-C catalyst suggests that the iron species, the presence of which had been confirmed by XRF and XPS, were likely present in either an amorphous or even "mononuclear" form, possibly involving coordination with other species that survived the pyrolysis and acid leach.

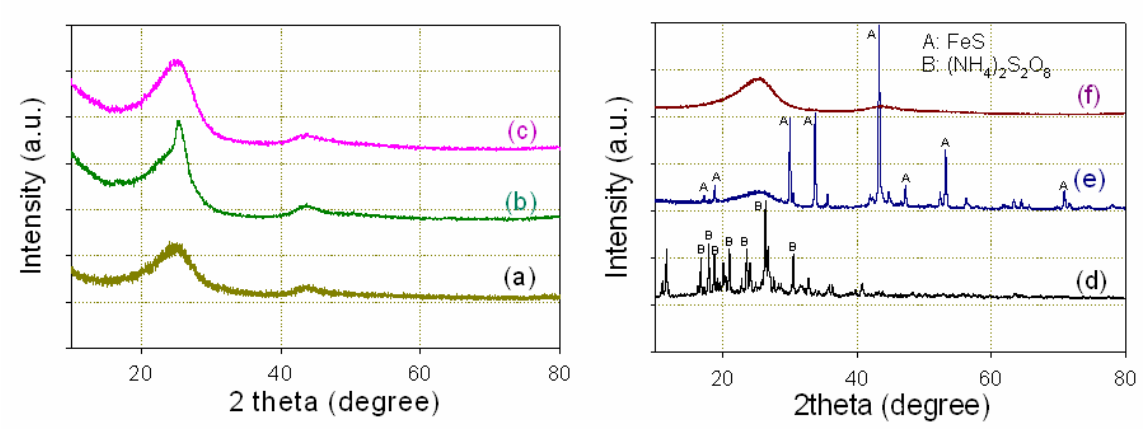

Figure 8. XRD patterns for various support/catalyst samples: (a) as-received carbon black; (b) pyrolyzed carbon black; (c) PANI-C; (d) PANI-Fe-C, before pyrolysis; (e) PANI-Fe-C, after pyrolysis but before chemical treatment; (f) PANI-Fe-C, after chemical treatment.

As mentioned earlier, the nature of the active ORR site on non-precious catalysts of the type investigated in this work has been the subject of an ongoing controversy for quite some time. In particular, a number of authors have suggested that transition metals are not part of the active site and thus are not directly involved in the ORR. Since, however, the presence of metal in the precursor(s) does is required for making the most active catalysts, the interpretation assigns such metals as Fe or Co a secondary role in the active-catalyst synthesis. That role is to promote the formation stable N-containing sites on the carbon substrate and, also, edge planes of carbon, which have been claimed to participate in the active ORR sites. Many authors found no correlation between the activity and amount of metal species present, nor any evidence of the formation of Me-N moieties.

In this work, however, we found an XPS, XRD, and HRTEM evidence for the presence of transition metals on the catalyst surface and their interaction with both nitrogen and carbon structures. We also demonstrated a direct impact of the metal content on electrocatalytic activity. Consequently, we cannot solely assign the ORR activity of PANI-derived catalysts to nitrogen-doped carbon structures. While sites with more complex coordination of the metal ions in the form of pyrrolic and/or pyridinic species appears likely, the ultimate confirmation of their presence cannot be made without using highly advance surface analysis techniques.

Conclusions

New polyaniline-derived non-precious cathode catalysts, obtained by pyrolyzing carbon-supported PANI-complexes of Fe and Co, show good activity and stability in oxygen reduction in aqueous electrolyte at the PEFC cathode. The onset and half-wave potential of oxygen reduction in 0.5 M H_2SO_4 electrolyte can be as high as 0.90 and 0.77 V, respectively. RDE testing also reveals a well-defined mass-transport-limited current that attests to high density of the ORR active sites. The best performing catalysts can effectively reduce oxygen to water, at negligible H_2O_2 yields (0.4 % at 0.40 V). PEFC data confirm high ORR activity of PANI-derived catalysts, both in air and oxygen testing. The catalysts offer promising stability under fuel cell operating conditions, so far demonstrated for 450 hours in a hydrogen-air fuel cell.

While the nature of the active ORR site remains uncertain at this point, some preliminary data indicate possible involvement of metals in the oxygen reduction process. Pyrrolic and/or pyridinic species, coordinated to metal ions, may be at least partially responsible for the catalytic activity in this case.

Acknowledgments

Financial support of the DOE-EERE Hydrogen, Fuel Cells and Infrastructure Technologies Program as well as Los Alamos National Laboratory through Laboratory-Directed Research and Development program (LDRD) is gratefully acknowledged.

References

1. R. Jasinski, *Nature*, **201**, 1212 (1964).
2. D. Villers, X. Jacques-Bédard and J. P. Dodelet, *J. Electrochem. Soc*., **151**, A1507 (2004).
3. R. Bashyam and P. Zelenay, *Nature,* **443**, 63 (2006).
4. M. Bron, J. Radnik, M. Fieber-Erdmann, P. Bogdanoff and S. Fiechter, *J. Electroanal. Chem.,* **535**, 113 (2002).
5. M. Lefevre, J. P. Dodelet and P. Bertrand, *J. Phys. Chem. B*, **104**, 11238 (2000**)**.
6. M. Lefevre, J.P. Dodelet and P. Bertrand, *J Phys. Chem. B*, **109**, 16718 (2005).
7. S. Maldonado and K. J. Stevenson, *J. Phys. Chem. B*, **108**, 11375 (2004).
8. P. H. Matter, E. Wang and U. S. Ozkan, *J. Catal*., **243**, 395 (2006).
9. V. Nallathambi, J. W. Lee, S. P. Kumaraguru, G. Wu and B. N. Popov, *J. Power Sources*,**183**, 34 (2008).
10. G. A. Rimbu, C. L. Jackson and K. Scott, *J. Optoelectron. Adv. Mater.*, **8**, 611 (2006).
11 S. L. Gojkovic, S. Gupta and R. F. Savinell, *Electrochim. Acta*, **45**, 889 (1999)**.**
12 H. Wang, R. Cote, G. Faubert, D. Guay and J. P. Dodelet, *J. Phys. Chem. B*, **103**, 2042 (1999).
13 J. R. Pels, F. Kapteijn, J. A. Moulijn, Q. Zhu and K. M. Thomas, *Carbon*, **33**, 1641 (1995).
14 J. Murayama and I. Abe, *Electrochim. Acta*, **48**, 1443 (2003).
15 L. Zhang, J. Zhang, D. P. Wilkinsona and H. Wang, *J. Power Sources*, **156**, 171 (2006).

16 G. Wu, L Li, J. H. Li and B. Q. Xu, *Carbon*, **43**, 2579 (2005).
17 A. Widelov and R. Larsson, *Electrochim. Acta*, **37**, 187 (1992).
18 J. M. Jones, Q. Zhu and K. M. Thomas, *Carbon*, **37**, 1123 (1999).
19 A. J. Heod, T. C. Gibb, A. A. Herod, B. Xu, S. Zhang and R. Kandiyoti, *Fuel*, **75**, 437 (1996).
20 E. Claude, T. Adduo, J. Latour and P. Aldebert, *J. Appl. Electrochem*., **28**, 57 (1998).
21 G. Faubert, R. Cote, D. Guay, J. P. Dodelet, G. Denes and P. Betrand, *Electrochim. Acta*, **43**, 341 (1998).
22 A. L. Bouwkamp-Wijnholtz, W. Visscher, J. A. R. Van Veen, E. Boellaard, A. M. Van der Kraan and S. C. Tang, *J. Phys. Chem. B,* **106,** 12993 (2002).
23 M. Lefèvre, J. P. Dodelet and P. Bertrand, *J. Phys. Chem. B* **106** 8705 (2002).
24 J. A. R. Van Veen, H. A. Colijn and J. F. Van Baar, *Electrochim. Acta,* **33** 801 (1988).
25 S. B. Yang, H. Q. Hu and G. H. Chen, *Carbon,* **40,** 277 (2002).
26 H. E. King and C. T. Prewitt, *Acta Crystallogr. B,* **38**, 1877 (1982).